



	<b>Experiment title:</b> Investigation of the storage capacity of novel all-solid-state oxygen ion batteries by in situ X-ray absorption spectroscopy	<b>Experiment number:</b> MA 5239
<b>Beamline:</b> ID12	<b>Date of experiment:</b> from: 28.06.2022 to: 04.07.2022	<b>Date of report:</b> 14.12.2022
<b>Shifts:</b> 18	<b>Local contact(s):</b> Fabrice Wilhelm, wilhelm@esrf.fr	<i>Received at ESRF:</i>
<b>Names and affiliations of applicants</b> (* indicates experimentalists): Alexander Stangl <sup>1</sup> , Alexander Schmid <sup>2</sup> , Martin Krammer <sup>2</sup> , Fjorelo Buzi <sup>3</sup> , Adeel Riaz <sup>1</sup> , Andreas Nenning <sup>2</sup> , Federico Baiutti <sup>3</sup> , Carmen Jiménez <sup>1</sup> and Mónica Burriel <sup>1</sup> <sup>1</sup> Université Grenoble Alpes, CNRS, Grenoble INP, LMGP, Grenoble F-38000, France <sup>2</sup> Institute of Chemical Technologies and Analytics, Vienna University of Technology, Getreidemarkt 9, Vienna, 1060, Austria <sup>3</sup> Catalonia Institute for Energy Research (IREC), Barcelona 08, Spain		

## Report:

### 1. Objective:

The objective of this experiment was to gain insight in the oxygen storage capacity of potential electrode materials of a new type of all-solid state oxygen ion battery. Therefore, the oxidation state of Fe, Ni and Co in the electrode materials (La,Sr)FeO<sub>3-δ</sub> (LSF), La<sub>2</sub>NiO<sub>4+δ</sub> (LNO) and (La,Sr)CoO<sub>3-δ</sub> (LSC), respectively was measured using XANES. For each material, measurements were performed in (i) thin film reference samples and (ii) thin film devices using a special electrode geometry under various electrical polarisations and different temperatures (*e.g. in situ* conditions).

### 2. Experimental

The photon source is the APPLE-II type helical undulator HU-38 at the fundamental harmonic of its emission. Reference samples were measured in the 2<sup>nd</sup> experimental hutch (EH3) under vacuum and at T = 298K in a top-up 7/8+1 multibunch filling mode for better beam stability and nearly constant beam current of 200 mA, with injections every hour. The intensity detector used was a silicon photodiode and the total fluorescence yield (TFY) was collected in backscattered geometry (detector plane at 90° respect the beam vector).

The *in situ* measurements were performed in oxygen atmosphere (1atmo) using a temperature cell (Nextron), equipped with 6 tips for electrical contacts and a Kapton window. A schematic of the electrochemical device architecture, used for *in* and *ex situ* polarisation measurements, is shown in Figure 1(a-c), consisting of two partly burried Pt top electrodes (connected with either 0, 1 or 3 thin Pt bridges), the oxide thin film and a 100nm thick ZrO<sub>2</sub> capping layer on top of a YSZ single crystal substrate with a Pt-infiltrated (Ce,Gd)O<sub>2</sub> back electrode, which is short-circuited to the grounded top electrode. Two silicon drift detectors<sup>1</sup> were used to collect the partial fluorescence yield (PFY) in backscattering configuration. A thin (10-20μm) Mn, Fe, or Co foil was inserted in front of the SDD to reduce elastic scattering for Fe, Co and Ni K-edge measurements, respectively. A beam spot size of ~200 μm was set with the secondary slits and it was used for low-photon density XANES over large

<sup>1</sup> Each silicon drift detector is a SiriusSD with an on-chip active area of 100 mm<sup>2</sup> equipped with a low capacitance primary amplification device (RaySpec) coupled to Falcon-X processors (XIA LLC).

areas. Polyscans were performed in narrow energy ranges around the adsorption edge positions of Fe, Ni and Co. For time-resolved measurements, the beam was fixed at an energy close to the K-edge inflection points and intensity was followed over time. A Keithley 2410 sourcemeter was used to polarise the battery devices and establish a lateral oxygen gradient within the thin film.

### 3. Results:

For each of the three oxide materials, a set of 5 samples was studied, as outlined in Table 1. The oxide film thickness was 200nm. For the *ex situ* measurement, an oxygen chemical potential gradient was frozen into the device by quenching it from 400°C in O<sub>2</sub> atmosphere under applied voltage to room temperature.

			Structure
Reference thin film samples	as grown		oxide/YSZ
	reduced	400°C, humidified H <sub>2</sub>	
	oxidized	400°C, O <sub>2</sub>	
Electrochemical devices	<i>ex situ</i>	400°C, O <sub>2</sub> , under bias	ZrO <sub>2</sub> /oxide/Pt/YSZ/Pt-(Ce,Gd)O <sub>2</sub>
	<i>in situ</i>		

Table 1: Overview of 5 studied samples for each oxide material: LSF, LSC, LNO

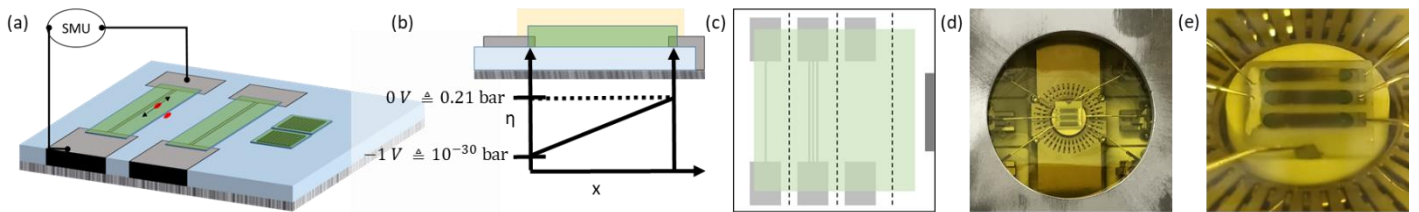


Figure 1: Electrochemical device configuration for *in situ* polarization measurements and its cross section (b), indicating linear decay of applied potential,  $\eta$ , and corresponding effective  $pO_2$ . Schematic top view of sample containing 3 devices with 1, 3 and 0 Pt bridges between the Pt electrodes. (d) Image of setup with loaded sample during beam time. (e) Top device under polarisation with visible oxygen gradient due to changes in transparency.

#### La<sub>0.6</sub>Sr<sub>0.4</sub>FeO<sub>3-δ</sub> (LSF)

In a first experiment the frozen oxygen gradient was mapped using X-ray absorption spectroscopy at room temperature (*ex situ*). Spectra of the Fe K-edge were recorded at different positions on the sample along the voltage gradient. Two features of these spectra were analysed: The inflection point of the absorption edge (see Figure 2a) and the position of the relative maximum at energies below the absorption edge, see Figure 2b. The position shift of these features are shown in Figure 2c. The position of the pre-edge maximum and the inflection point both shift with polarization by -0.65 and -0.45 eV, respectively. Despite the different magnitude of the shift, both features show the same dependence on voltage: Both features shift very little between 0 and -0.1 V, followed by a steep decrease between -0.1 and -0.35 V and a 2<sup>nd</sup> plateau between -0.35 and -0.8 V. The energies of both plateaus agree well with the energies measured in the reference samples, where the oxygen non-stoichiometry  $\delta$  of LSF thin films is well known, *e.g.* equals 0 for the oxidised and 0.2 for the reduced film. This confirms that by applying a voltage we can reduce the sample from  $\delta = 0$  (at 0 V) to  $\delta = 0.2$  (below -0.35 V).

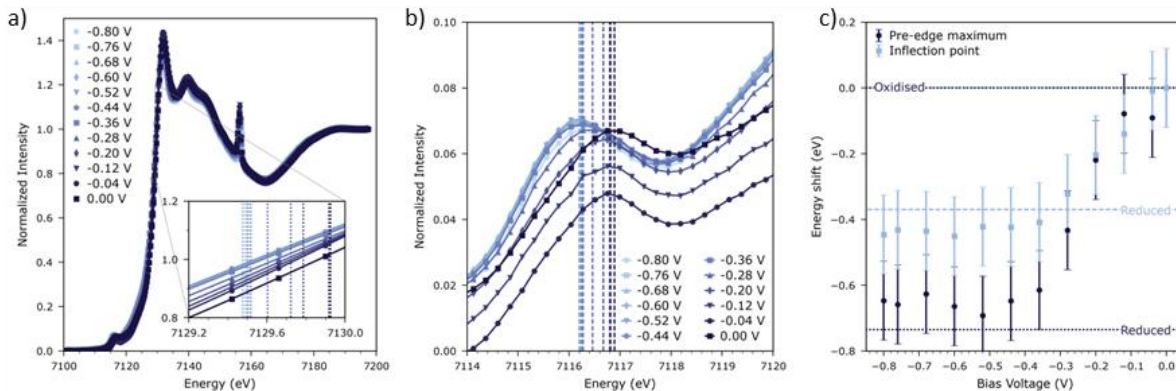


Figure 2: X-ray absorption spectra around the Fe K-edge with magnified inflection point (a), and pre-edge maximum (b). The shift in energy position of these features under voltage, extracted from (a) and (b) is shown in (c) together with reference samples.

In the second experiment a voltage gradient was applied at 400 °C in a pure oxygen atmosphere and the sample was characterized under these conditions *in-situ*. The results obtained from this *in-situ* measurement of the gradient (not shown here) were similar to those measured on the ex-situ sample, with an oxygen window of  $\Delta\delta\approx 0.2$  at elevated temperature. **The capacity of such oxygen ion battery electrode therefore accounts to about 50mAh/g (300mAh/cm<sup>3</sup>).**

To investigate the kinetics of the oxygen non-stoichiometry variation (*e.g.* charging characteristics), voltage steps from 0 to -0.6 V and from -0.6 to 0 V were applied to the sample and the absorption was then measured as a function of time at different temperatures. Rather than recording full spectra, the intensity at one single energy (7129.7 eV, at the absorption edge inflection point) was measured continuously, see Figure 3a and Figure 3b. From these time series time constants were extracted by fitting the data to a single exponential. These time constants were then fitted to an Arrhenius equation to estimate the activation energies of underlying electrochemical processes, see Figure 3c. Activation energies of 1.1 and 0.3 eV were estimated for the forward (0 to -0.6 V) and reverse (-0.6 to 0 V) steps.

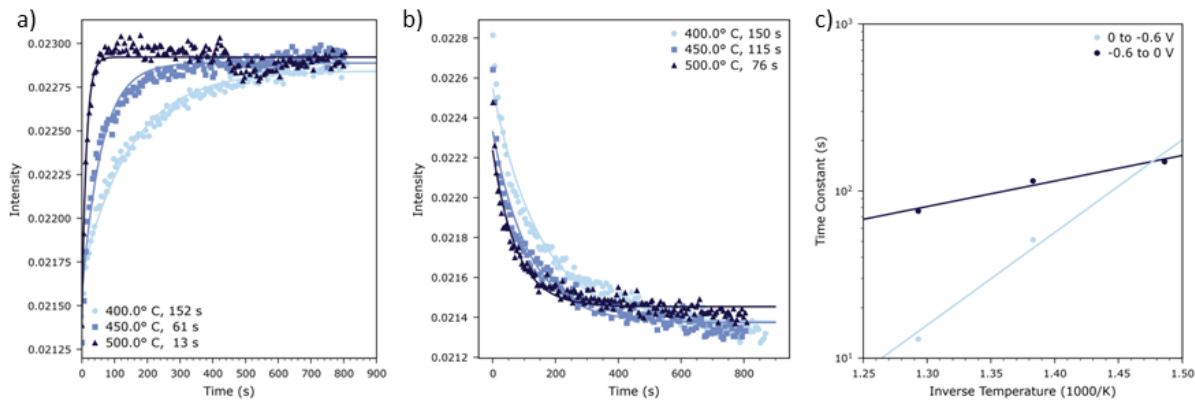


Figure 3: Intensity at 7129.7 eV vs. time after application of a -0.6 V step (a) and after a step back to 0 V (b). Extracted time constants are shown in (c) in an Arrhenius plot.

Lastly, the build-up of the stoichiometry gradient was studied as a function of time and voltage between the gradient endpoints to define the operation window of a potential oxygen battery. Figure 4a shows the intensity at the polarized endpoint of the gradient vs. time for different endpoint voltages. Essentially, a notable stoichiometry gradient first emerges at -0.3 V and is fully established at -0.5 V. This is in good agreement with the results obtained on the ex-situ characterized sample. Figure 4b shows the incremental build-up of a spatial gradient with increasing voltage at the gradient end points. Figure 4c shows the same curves normalized to the voltage at the respective spatial positions. The excellent agreement of the individual data confirms that with this sample design we establish a defined linear potential gradient along our sample and thus validates the experiment design.

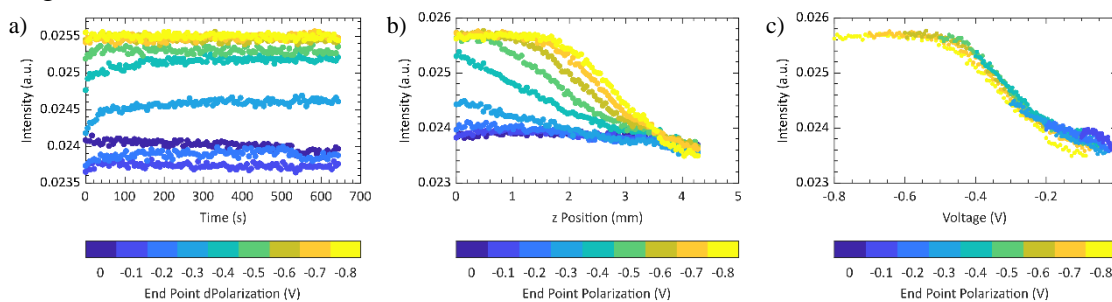


Figure 4: a) Intensity vs. time after application of different voltages. b) Spatial gradients for different voltages. c) Intensity vs. voltage for different maximum voltages.

### **La<sub>0.6</sub>Sr<sub>0.4</sub>CoO<sub>3-δ</sub> (LSC)**

The valance state of Co was studied to gain insight into the oxygen vacancy concentration changes in LSC. Reference thin film samples annealed under different conditions show only a small shift of about 0.15eV, see Figure 5a. Equivalent to measurements in LSF, *in situ* measurements were performed at 400°C in flowing O<sub>2</sub>. Full spectra under different polarizations were obtained at the biased end point of the device. Details around the

edge position are shown in Figure 5b, with the derivative in the inset. For the highest polarization of  $-0.8\text{eV}$  we observe a shift of about  $-0.6\text{eV}$ , which corresponds to  $\delta \approx 0.2$ , and similarly to LSF a **capacity of about  $50\text{mAh/g}$** . The edge shift as a function of applied bias was directly followed by measuring the intensity at fixed energy ( $E=7726.14\text{eV}$ ) and using a rigid shift model, shown in Figure 5b (highlighted within red frame) and as function of the bias in Figure 5c. The edge shift follows an S shaped curve, with saturation within the shown voltage range. The light blue shaded area corresponds to the error in the determination of the absorption edge shift due to changes in the slope around the inflection point with bias. However, the tendency of the shift follows the trend of the shift obtained by full reference scans (red markers).

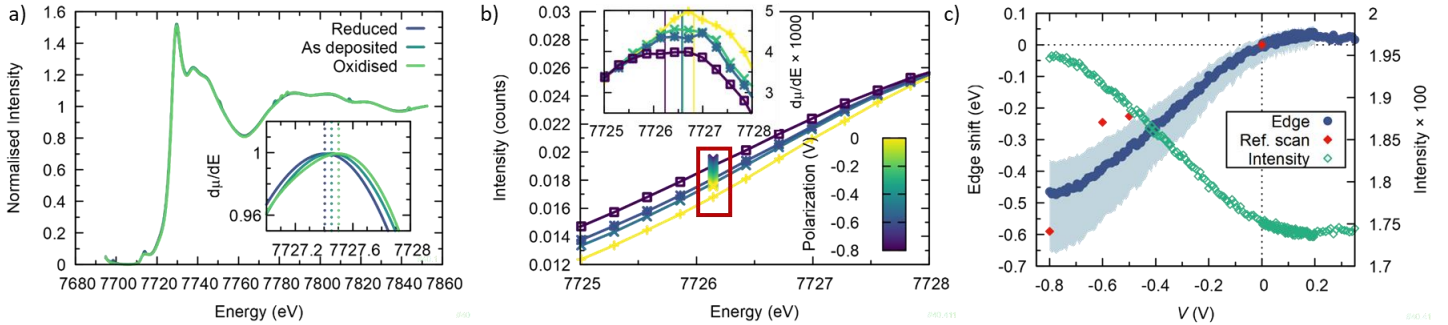


Figure 5: a) LSC reference thin films, inset shows normalised derivative. b) *In situ* XAS measurements at different polarization (solid lines correspond to 0,  $-0.5$ ,  $-0.6$  and  $-0.8\text{V}$ ), with the derivative in the inset. c) Intensity of inflection point at polarized end point as function of applied polarization and calculated edge shift using rigid shift model. Red diamonds correspond to shift obtained by full reference scans in b).

### $\text{La}_2\text{NiO}_{4+\delta}$ (LNO)

While in LSF and LSC oxygen non-stoichiometry is due to the formation of oxygen vacancies, the main defects in LNO are oxygen interstitials. We have investigated the solubility of excess oxygen via reference annealings under different atmospheres and *in situ* via an electrical driving force. The energy shifts for about  $0.6\text{eV}$  from the reduced state with  $\delta=0.06$  to the oxidised state with a larger oxygen off-stoichiometry of  $\delta=0.16$ , as shown in Figure 6a. A similar shift is obtained *in situ* under a polarization of  $-0.8\text{V}$  in oxygen atmosphere, which proves that effective and real  $p\text{O}_2$  are equivalent as driving force for changes in the oxygen stoichiometry and therefore as mechanism to charge and discharge the electrode within a battery cell.

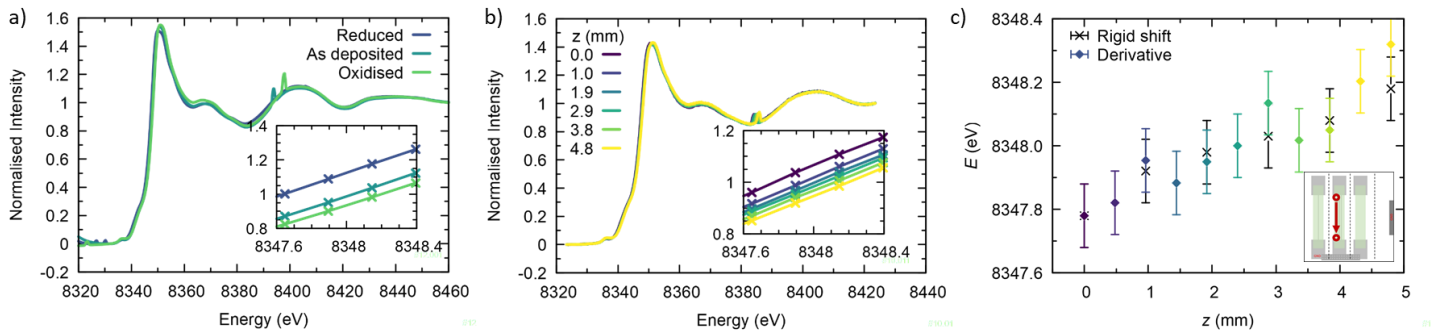


Figure 6: a) LNO thin film reference samples after different annealing treatments at RT. b) *In situ* XAS spectra at  $400^\circ\text{C}$  under polarization ( $-0.8\text{V}$ ) along voltage gradient and c) extracted shift in adsorption edge.

In contrast to LSF, we did not find a plateau of constant energy nor sharp transitions between 0 and  $-0.8\text{eV}$ . Crystallographically speaking, the limit for oxygen interstitials in LNO is  $\delta_{\text{max}}=2$ , while experimentally only about 10% can be filled under atmospheric pressure. To analyse the oxygen off-stoichiometry window the voltage was swept between  $-1.2\text{V}$  and  $+1\text{V}$ , while the intensity was constantly recorded at the inflection point energy, see Figure 7a. Applying the rigid shift model one obtains the edge shift, shown in Figure 7b, where a S-curved transition can be observed within the set V range, with saturation below  $-1\text{V}$  and above  $+0.6\text{V}$ . The energy window accounts to about  $0.9\text{eV}$  and thus  $\Delta\delta \approx 0.15$ , which results in an **oxygen storage capacity of about  $20\text{mAh/g}$  ( $150\text{mAh/cm}^3$ )**. The observed hysteresis in the branch of decreasing voltage is likely caused by kinetic effects, as the measurements were performed out of equilibrium. The oxide needs a finite time to counterbalance the applied voltage by changing its oxygen stoichiometry, as can be seen in Figure 7c. The time constants vary significantly for LSF and LNO and are therefore likely related to oxygen transport mechanism relevant to charging and discharging behaviour, rather than oxygen diffusion through the YSZ layer, as well as oxygen reduction and evolution reactions on the porous Pt-CGO back electrode.

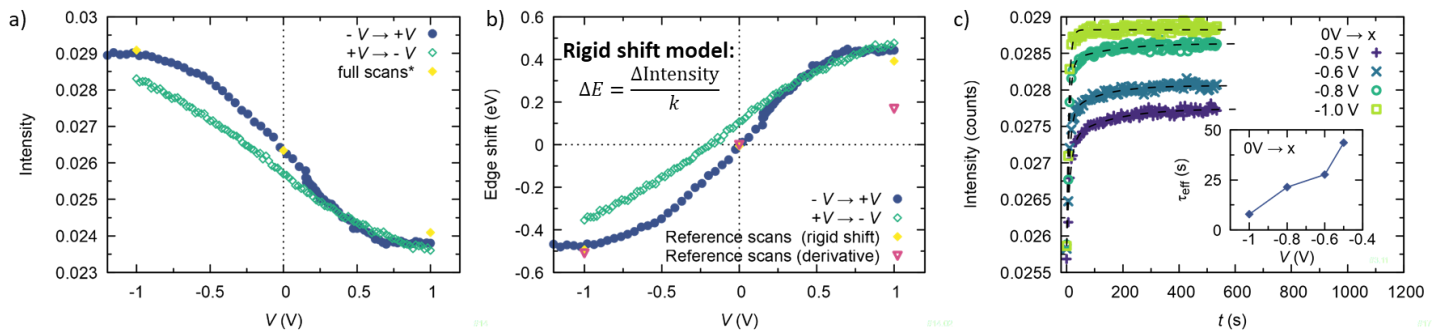


Figure 7: a) Intensity of LNO inflection point at 8348.15 eV upon voltage sweep and b) calculated edge shift using the rigid shift model. c) Kinetic measurements at 400°C.

#### 4. Conclusions:

XANES measurements were performed on three different electrode materials for a new type of solid state oxygen ion battery. The oxygen off-stoichiometry is the crucial parameter for the potential capacity of such a device and thus was investigated under *ex situ* and *in situ* conditions. Comparison with *ex situ* annealed reference films allowed to relate bias induced changes in the absorption spectra to modifications of the oxygen defect densities, such as vacancies and interstitials, and hence proved the equivalence of effective and real  $pO_2$  conditions. It was shown, that in all three oxides the oxygen non-stoichiometry can be electrochemically tuned within a  $\delta$  range of 0.15-0.2, leading to capacities of 20-50mAh/g (150-300mAh/cm<sup>3</sup>) at operation temperatures between 400 and 500°C. Charging and discharging characteristics were studied as function of temperature and applied polarization using time resolved XAS measurements at constant energy. Extracted time constants show Arrhenius type behaviour and varied 1-2 orders of magnitude between different materials, which indicates that they are related to oxygen transport mechanism within the oxide and thus relevant to battery performance. Overall, this proof of concept study showed that LSF, LSC and LNO are promising oxide materials for the integration into a novel battery family, which is envisaged to show long lifetime, reduced environmental impact and avoid toxic and hazardous materials.